Scilight

Renewable Chemistry

https://www.sciltp.com/journals/rc

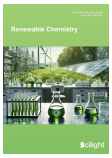

Article

Pyrolysis of Woody Biomass Loaded with Phytic Acid in a Fluidized-Bed Reactor for Producing Levoglucosenone

Tsinjo Nirina Rafenomananjara [1], Shinji Kudo [1,2,*], Chihiro Asano [1], Ren Akai [1], Yasuyo Hachiyama [2] and Jun-ichiro Hayashi [1,2]

[1] Interdisciplinary Graduate School of Engineering Sciences, Kyushu University, 6-1 Kasuga Koen, Kasuga 816-8580, Japan
[2] Institute for Materials Chemistry and Engineering, Kyushu University, 6-1 Kasuga Koen, Kasuga 816-8580, Japan
* Correspondence: kudo.shinji.641@m.kyushu-u.ac.jp

How To Cite: Rafenomananjara, T.N.; Kudo, S.; Asano, C.; et al. Pyrolysis of Woody Biomass Loaded with Phytic Acid in a Fluidized-Bed Reactor for Producing Levoglucosenone. *Renewable Chemistry* **2025**, *1*(1), 6. https://doi.org/10.53941/rc.2025.100006

Received: 11 October 2025
Revised: 13 November 2025
Accepted: 19 November 2025
Published: 27 November 2025

Abstract: Efficient conversion of lignocellulosic biomass into high-value chemicals remains challenging due to its complex structure. The selective production of levoglucosenone (LGO), a valuable bio-based building block derived from cellulose, has attracted increasing attention as part of efforts to establish sustainable chemical feedstocks. In this study, the continuous pyrolysis of woody biomass for LGO production was conducted using a fluidized-bed pyrolyzer, which is generally employed for bio-oil production but has not yet been tested for this reaction. Phytic acid (PA), a naturally occurring organic phosphorus compound abundant in agricultural residues, was employed as a biogenic catalyst and loaded over biomass. The pyrolysis characteristics were investigated in terms of LGO yield under various operating conditions of the fluidized-bed. Prior to PA loading, the removal of alkali and alkaline earth metals from feedstock biomass via oxalic acid-washing was examined to improve anhydrosugars yields. Thermogravimetric analysis (TGA) revealed that PA loading lowered the temperature of biomass pyrolysis and increased char yield, confirming its catalysis toward dehydration. TGA of model compounds of biomass components indicated PA catalyzed only cellulose pyrolysis, while it did not affect that of hemicellulose and lignin. In the continuous pyrolysis experiments, the best conditions achieved an LGO yield of 6.3 wt% (17.1 wt% on a cellulose basis) at an average bed temperature of 300 °C. The results demonstrate, for the first time, that a biogenic phosphorus catalyst such as PA can effectively promote LGO formation under continuous fluidized-bed operation. The study also provides fundamental insights for key factors affecting the LGO yield during steady-state operation of the fluidized-bed, such as the thermal stability of LGO and its interaction with char.

Keywords: lignocellulosic biomass; pyrolysis; phytic acid; levoglucosenone; fluidized-bed

1. Introduction

Research and technological development toward carbon-neutral societies have intensified worldwide. In the energy sector, multiple renewable options, such as solar, wind, and hydrogen, are being implemented. In contrast, replacing fossil-derived chemical feedstocks relies almost exclusively on biomass resources. Although significant progress has been made in the utilization of biomass for chemical production, most commercialized technologies still depend on first-generation feedstocks such as starch and vegetable oils, which compete with food supply [1]. In the long term, lignocellulosic biomass is expected to play a crucial role owing to its abundance and renewability.

Copyright: © 2025 by the authors. This is an open access article under the terms and conditions of the Creative Commons Attribution (CC BY) license (https://creativecommons.org/licenses/by/4.0/).
Publisher's Note: Scilight stays neutral with regard to jurisdictional claims in published maps and institutional affiliations.

In Japan alone, about 100 million tons of woody biomass (~50 million tons of carbon) is estimated to be sustainably harvested each year [2], far exceeding the amount of petrochemical naphtha (≈40 million kL) used currently as chemical feedstock [3]. Therefore, the utilization of woody biomass as a chemical feedstock is rational, and the development of relevant technologies is of great importance.

However, lignocellulosic biomass is a complex matrix composed of strongly cross-linked macromolecules such as cellulose, hemicellulose, and lignin, which makes its high-value conversion technically challenging. Numerous studies have attempted to fractionate and convert these components individually, often via hydrothermal or acid-catalyzed wet processes. Despite their effectiveness, such methods face limitations in productivity and cost efficiency. Pyrolysis offers an attractive alternative due to its simplicity and fast reaction rates. Among the volatile products from pyrolysis, cellulose-derived anhydrosugars, levoglucosan (LGA) and levoglucosenone (LGO) are notable because of their availability. In particular, LGO possesses two chiral centers and six differently functionalized carbons, which are useful as feedstock for the synthesis of a green solvent, drug candidate chemicals, and polymers [4–7].

Efficient LGO production requires catalysis for cellulose dehydration during pyrolysis. Depending on the catalytic target and reaction conditions, three main approaches have been explored [8]: (i) loading molecular or liquid catalysts, such as mineral acids and ionic liquids, over biomass prior to pyrolysis [9–11], (ii) reforming of volatiles, mainly LGA, over solid catalysts [12–15], and (iii) catalytic conversion of biomass or bio-oil in the liquid phase [16–18]. The FURACELL process developed by Circa Group exemplifies the first approach, employing phosphoric acid as the catalyst and sulfolane to achieve commercial scale LGO production [19]. Phosphoric acid has long been known as a highly active molecular catalyst for LGO formation [20–22]. However, phosphoric acid is produced by energy-intensive wet-process from finite phosphate rock. As phosphate demand is projected to exceed supply by 2040 [23], sustainable alternatives are required. Recently, our group reported that phytic acid (PA), a natural phosphorus compound abundant in agricultural wastes, exhibits catalytic activity comparable to or even greater than phosphoric acid on a phosphorus-basis, achieving up to 20 wt% LGO yield from pure cellulose using a fixed-bed pyrolyzer [24].

Despite many advances in catalyst development, few studies in literature have addressed the continuous production of LGO. Most reported systems employ analytical pyrolyzers for milligram-scale tests or semi-batch reactors for gram-scale experiments. The commercial process mentioned above has used a screw-conveyer type pyrolyzer for the continuous LGO production [25]. According to the mass balance presented in their report, the yield of LGO was estimated to be around 6 wt% [8]. Dobele et al. also used the same type of pyrolyzer and achieved the yield of LGO at 6.5 wt% from woody biomass loaded with 5 wt% of phosphoric acid [26]. Using a semi-batch type pyrolyzer, Li et al. continuously supplied feedstock biomass mixed with solid catalysts for 5 min to a quartz wool fixed bed in a reactor tube and obtained LGO with the yield of 21 wt% from pure cellulose [12].

Fluidized-bed pyrolyzers are often used for bio-oil production. This pyrolyzer enables fast heating of biomass through solid-solid contact with preheated bed material, which makes use of the characteristics of pyrolysis, the fast reaction, and is, therefore, ideal for continuous operation. Fast heating suppresses char formation, improving the yield of volatiles. Several studies have demonstrated continuous LGA production using fluidized beds [27–29]. We also have reported continuous LGA production with the yield of about 30 wt% on a cellulose basis from woody biomass [30]. In the study, the removal of alkali and alkaline earth metallic species (AAEMs), which are known to catalyze the decomposition of the pyranose ring of cellulose during the pyrolysis [31], from the feedstock with acid-washing pretreatment was effective for improving LGA yields. As such, fluidized-bed pyrolyzers are useful for pyrolysis of biomass, but to the best of our knowledge, LGO production with this reactor has not yet been reported.

The present study aims to evaluate the continuous production of LGO through the pyrolysis of PA-loaded woody biomass in a fluidized-bed reactor. First, the effect of organic acid-washing pretreatment on pyrolysis was examined. Second, thermogravimetric analysis was performed to elucidate the influence of PA loading on the pyrolysis characteristics. Finally, continuous pyrolysis experiments were conducted to investigate how operating parameters, such as PA loading and temperature, affect LGO yield in a fluidized-bed pyrolyzer.

2. Experimental

2.1. Materials

Japanese cedar (CD), a softwood, was used as the woody biomass feedstock. Air-dried CD chips were crushed using a cutter mill and sieved to obtain particles within 0.36–1.0 mm. For model compound analysis, microcrystalline cellulose (Merck), xylan from beech wood (Tokyo Chemical Industry, Merck, Darmstadt, Germany), and alkali lignin (Merck, Darmstadt, Germany) were employed. Oxalic acid and phytic acid (50% aqueous solution) were purchased from FUJIFILM Wako Pure Chemical Corporation (Osaka, Japan). The

elemental composition of CD was C 49.8 wt%, H 6.4 wt%, N 0.3 wt%, and O 43.8 wt% on a dry and ash free basis. The chemical composition was cellulose 35.4 wt%, hemicellulose 15.8 wt%, lignin 35.3 wt%, extractives 5.7 wt%, and ash 1.0 wt% [30].

2.2. Pretreatments

Two pretreatment steps were applied to the CD samples: organic acid-washing and PA loading. Oxalic acid was selected as the organic acid. In a typical experiment, CD was added to 0.5 M aqueous oxalic acid at solid:liquid mass ratio = 1:20, and the slurry was stirred at room temperature for 3 or 12 h. After treatment, the sample was repeatedly washed with deionized water until the filtrate pH reached 6–7, filtered, and vacuum-dried overnight at 60 °C. After the acid-washing with 0.5 M oxalic acid for 12 h, the ash content of CD decreased to 0.18 wt%. Subsequently, 50 g of CD was added to 300 mL of aqueous solution containing PA at desired concentrations. The slurry was stirred and dried using a rotary evaporator to obtain PA-loaded CD. For TGA experiments with model compounds, PA loading was carried out by freeze-drying to avoid altering the feedstock chemical structure during drying. PA contents were adjusted to 0.3 wt% for cellulose and 1.0 wt% for xylan and lignin.

The chemical composition of CD was analyzed following a two-step hydrolysis method using concentrated and diluted sulfuric acid [32]. The ash obtained by low temperature combustion (600 °C) was dissolved in a mixed acid solution of 1 M HF and 1 M HNO_3, evaporated, and re-dissolved in methanesulfonic acid. The concentrations of AAEMs were quantified by ion chromatography using Shodex YS-50 column. The untreated CD contained 1.7, 0.42, and 1.5 g/kg-dry of K, Mg, and Ca, respectively. After acid washing, the cellulose content increased slightly to 36.6 wt%-dry.

2.3. Thermogravimetric Analysis (TGA)

TGA was performed using an STA7200 instrument (Hitachi High-Tech, Tokyo, Japan). 2 mg of sample was placed in a platinum pan, dried at 110 °C, and heated to 800 °C under N_2 flow (300 mL/min). The mass loss fraction, X, was determined on a dry basis. For CD samples, heating rates of 5, 10, and 20 °C/min were applied, and obtained data were analyzed using the distributed activation energy model (DAEM) reported by Miura and Maki [33].

2.4. Pyrolysis Experiments

The effect of acid-washing on pyrolysis was investigated using a fixed-bed pyrolyzer. 0.5 g of CD sample was placed in a quartz boat and heated under flowing N_2 (200 mL/min) in a quartz tube from room temperature to 500 °C at a rate of 10 °C/min, followed by isothermal holding for 10 min. The condensable volatiles (bio-oil) were collected using a cold trap and a subsequent filter trap. The system pressure was maintained at 10 kPa with a vacuum pump connected downstream of the filter trap. The recovered bio-oil was dissolved in acetone and analyzed using a gas chromatograph (Shimadzu (Kyoto, Japan), GC-FID) equipped with a GL Sciences TC-1701 capillary column. The yields of LGO and LGA were quantified based on calibration curves.

The thermal stability of LGO in gas phase was evaluated with a gas flow type tubular reactor equipped with two independently controlled electric furnaces. N_2 was supplied at 600 mL-SATP/min from the tube entrance. In the tube located upstream furnace, 50 mg of LGO placed in a platinum container was set and heated at 140 °C to generate a steady LGO vapor stream (≈0.4 mg/min) and feed to the downstream reactor for 120 min. The downstream furnace was maintained at temperatures between 200 and 400 °C. LGO in the outlet gas was condensed and analyzed as described above to determine its recovery.

Continuous pyrolysis experiments were carried out using a laboratory scale fluidized-bed reactor, schematically illustrated in Figure 1. The reactor consisted of a 40 mm i.d. stainless-steel tube packed with silica sand (100–200 μm, pre-calcined at 600 °C) as the bed material. N_2 introduced from the bottom passed sequentially through a layer of 5 mm zirconia balls (gas distributor), the fluidized bed, and the headspace before exiting from the upper outlet. The bed and headspace volumes were approximately 125 mL and 620 mL, respectively. The minimum fluidization velocity (U_{mf}) was 1.98×10^{-2} m/s, and the gas flow rate was adjusted to $3.4 \times U_{mf}$.

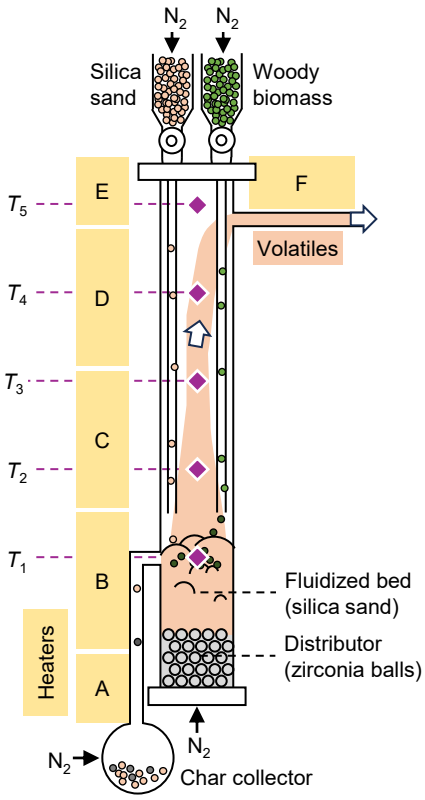

Figure 1. Schematic of the fluidized-bed pyrolyzer used in this study.

CD was continuously fed at 0.5 g/min using Micron Feeder (Aishin Nano Technologies (Saitama, Japan), CT series). The feedstock entered the reactor through a 6 mm i.d. tube and dropped into the fluidized bed from a height of ~170 mm above the static bed surface. Carrier N_2 at 700 mL-SATP/min was co-fed with CD. Two operational modes were employed: CD was fed alone in mode I, allowing char accumulation in the bed, and in mode II, CD and silica sand were co-fed at 0.5 and 1.5 g/min, respectively, with a char/sand outlet near the bed surface to maintain steady-state operation. In mode II, N_2 was also introduced from the sand feeder (200 mL-SATP/min) and the char collector (50 mL-SATP/min). The reactor was heated by six independently controlled electric furnaces (A–F). Furnaces A, E, and F were muffle heaters designed to fit the shape of the reactor, while B–D were three-zone type electric tubular furnace. Table 1 lists the set temperatures of each furnace. Thermocouples (T_1–T_5) monitored the temperature distribution (see Figure 1). T_1 was located ~10 mm below the static bed surface, and T_2–T_5 were spaced at 100 mm intervals. T_2–T_5 was measured just before the start of CD supply. T_1 was continuously measured during pyrolysis, and its average value was defined as $T_{1,ave}$. In a selected run, all temperatures from T_2–T_5 were measured throughout the pyrolysis.

Table 1. Set temperatures of heaters for fluidized-bed pyrolyzer.

Run	**1**	**2**	**3**	**4**	**5**	**6**	**7**	**8**	**9**	**10**	**11**	**12**	**13**	**14**
Heater	Temperature (°C)													
F	350	350	350	260	260	300	350	350	300	300	400	300	300	300
E	350	350	350	260	260	300	350	350	300	300	400	300	300	300
D	400	400	400	260	260	300	350	350	300	300	400	300	300	300
C	350	350	350	130	140	200	240	240	200	200	–	200	200	200
B	500	450	450	305	305	350	395	395	345	345	530	345	345	345
A	350	350	350	260	260	300	350	350	300	300	400	300	300	300

The condensable volatiles were recovered using a Liebig condenser (connected to the pyrolyzer outlet), followed by a cold trap and a silica filter. In some runs, non-condensable gases were analyzed on-line every 2.5 min using a micro-GC (Agilent (Santa Clara, CA, USA), 490 Micro GC) connected to the filter outlet. The collected char and bed material were calcined at 600 °C for 3 h in air, and the char yield was calculated from the mass loss.

The bio-oil samples were analyzed by GC-FID to quantify LGO and LGA, and by GC-MS (Shimadzu, QP-2020 NX) for compounds identification. The GC-MS was equipped with the same column (TC-1701) as the GC-FID. The oven temperature program was: 40 °C for 5 min; ramp at 5 °C/min to 250 °C; hold for 20 min. The

injection port, ion source, and transfer line temperatures were 280, 250, and 250 °C, respectively. For each sample, the 50 largest peaks were identified using the NIST library. The identified compounds were classified into five groups according to the following procedure: (1) compounds containing elements other than C, H, and O were categorized as others (O); (2) compounds containing a benzene ring were classified as aromatics (A); (3) compounds containing a furan ring were classified as furans (F); (4) sugars, including anhydrosugars, such as LGO and LGA, were classified as sugars (S); (5) the remaining compounds, most of which were light oxygenated compounds, were classified as L. Since more than 200 compounds were detected and quantifying all of them was difficult, semi-quantitative yields for each compound group were calculated according to Equation (1):

$$Y_i = \frac{\text{Total peak area of group } i}{\text{peak area of LGO}} Y_{\text{LGO}} \quad (1)$$

where Y_i represents the semi-quantitative yield of group i, and Y_{LGO} is the LGO yield (wt%). Total ion chromatograms were used for peak integration.

3. Results and Discussion

3.1. Acid-Washing Pretreatment

The presence of alkali and alkaline earth metals (AAEMs) in biomass strongly suppresses the formation of anhydrosugars such as LGA during pyrolysis and alters the composition of bio-oil [34]. Acid-washing pretreatments are therefore widely studied to remove these catalytic metals [35]. While mineral acids such as HCl and H_2SO_4 have been used effectively, they present environmental challenges, including corrosive effluent handling and incorporation of sulfur or chlorine species into the oil and char. Instead, as mentioned above, we recently showed the availability of oxalic acid for removing AAEMs [30]. Oxalic acid is a relatively strong organic acid, and its synthesis from CO_2 is also potentially feasible [36,37]. Herein, the effectiveness of oxalic acid-washing was explored in more detail.

Figure 2 shows the removal rate of K, Mg, and Ca under various oxalic acid concentrations. The solution pH ranged from 7 (pure water) to 0.8 (0.5 M oxalic acid). The AAEMs removal increased with increasing acidity, confirming that oxalic acid-washing effectively extracted AAEMs. Prolonging the treatment from 3 h to 12 h slightly enhanced removal efficiency. Potassium was removed more readily than divalent Mg and Ca, likely because the latter form stronger ionic bonds with functional groups (e.g., hydroxyls) in the biomass matrix. Although Ca and Mg oxalates have limited solubility in water, the enhanced removal at lower pH suggests that solubility limitations did not significantly affect the process under the present conditions. Pure-water washing alone was insufficient to substantially increase anhydrosugar yield [30]. These results indicate that oxalic acid concentration should be as high as practically feasible; however, its solubility in water at room temperature (≈1 M) sets an upper limit.

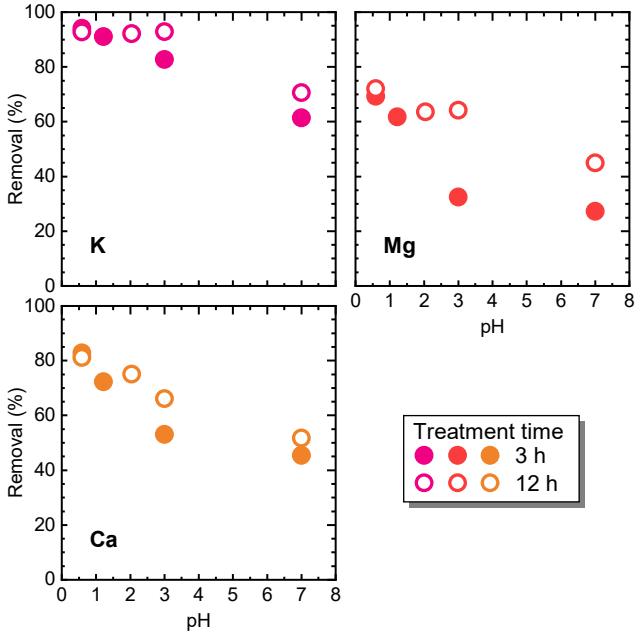

Figure 2. Removal of AAEMs (K, Mg, and Ca) during the acid-washing with oxalic acid aqueous solution at different concentrations.

Even under high oxalic acid concentrations, the removal of Mg and Ca remained incomplete. Nevertheless, as shown in Figure 3, the oxalic acid-washing produced a dramatic improvement in LGA yield (compare Control and Untreated at the top). The LGA yield exceeded 20 wt% on a cellulose basis, although it was lower than 35.3 wt% obtained from pure cellulose pyrolysis under the same conditions [30].

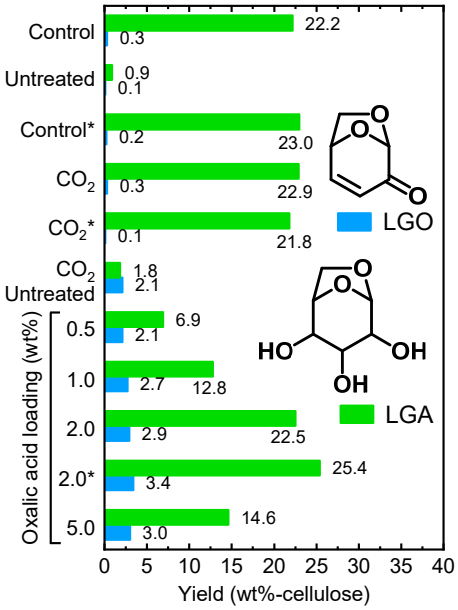

Figure 3. Yields of LGO and LGA during the pyrolysis of CD in fixed bed reactor. Control: 0.5 g CD, N_2 200 mL/min, 10 °C/min, final temperature 500 °C (holding time 10 min), 10 kPa. * indicates the pyrolysis was carried out at atmospheric pressure. In the "oxalic acid loading" experiments, oxalic acid was loaded over CD without acid-washing treatment.

Further experiments explored the influence of pyrolysis conditions. LGA released from the biomass matrix can undergo secondary condensation or polymerization reactions with char, reducing its recovery in bio-oil. Previous reports have shown that vacuum pyrolysis promotes LGA volatilization and improves yield from cellulose [11]. In this study, however, comparable yields were obtained even under atmospheric pressure. This can be attributed to the porous tracheid structure of softwood CD [38], which facilitates volatiles diffusion. Operating under ambient pressure is advantageous for fluidized-bed systems, simplifying process control. Changing the carrier gas from N_2 to CO_2 also had negligible influence on LGA yield. Since fluidized-bed pyrolysis generally requires high gas flow rates, the inert behavior of CO_2 suggests that recycled flue gas or CO_2-rich boiler off-gas could serve as carrier gas without yield loss.

In addition to acid-washing, impregnating biomass with inorganic acids can deactivate AAEMs through passivation, improving anhydrosugar yields [34]. Enhancement of the formation of 1,4:3,6-dianhydro-*α*-D-glucopyranose (DGP) from pyrolysis of cellulose when impregnated with equivalent or three times mass of oxalic acid has also been reported [39]. Here, oxalic acid was impregnated into CD to evaluate its effect on anhydrosugar production. Within the examined loading range, no selective formation of DGP was observed, but LGA yields markedly increased with acid loading up to 2 wt%. Excessive loading decreased yield, implying an optimum ratio between acid and AAEM content. The improvement is attributed to extraction and in-situ neutralization of AAEMs, followed by their re-precipitation in inactive forms, during the wet-impregnation. Thus, oxalic-acid impregnation can promote anhydrosugar formation, but it may also complicate the bio-oil composition through acid decomposition and could interfere with subsequent PA impregnation. From the findings and discussion above, in this study, acid-washing (0.5 M oxalic acid, 12 h) was adopted as the standard pretreatment. "CD" or "raw CD" hereafter refers to samples treated under these conditions.

3.2. TGA of PA-Loaded CD

TGA was performed to elucidate the effect of PA on the pyrolysis of CD. Figure 4a,b shows the results for raw CD and samples containing 1.0–4.0 wt% PA. For cellulose loaded with PA, overall pyrolysis temperature decreased markedly, while char yield increased, indicating catalytic promotion of dehydration and condensation [24]. A similar trend was observed for CD. The char yield increased from 14.5 wt% for raw CD to 35.6 wt% and 45.0 wt% for 1.0

wt% and 4.0 wt% PA loadings, respectively. The peak temperature (corresponding to maximum d*X*/d*t*) shifted from 369 °C to 239 °C as PA loading increased to 4.0 wt%, clearly demonstrating the catalytic effect of PA.

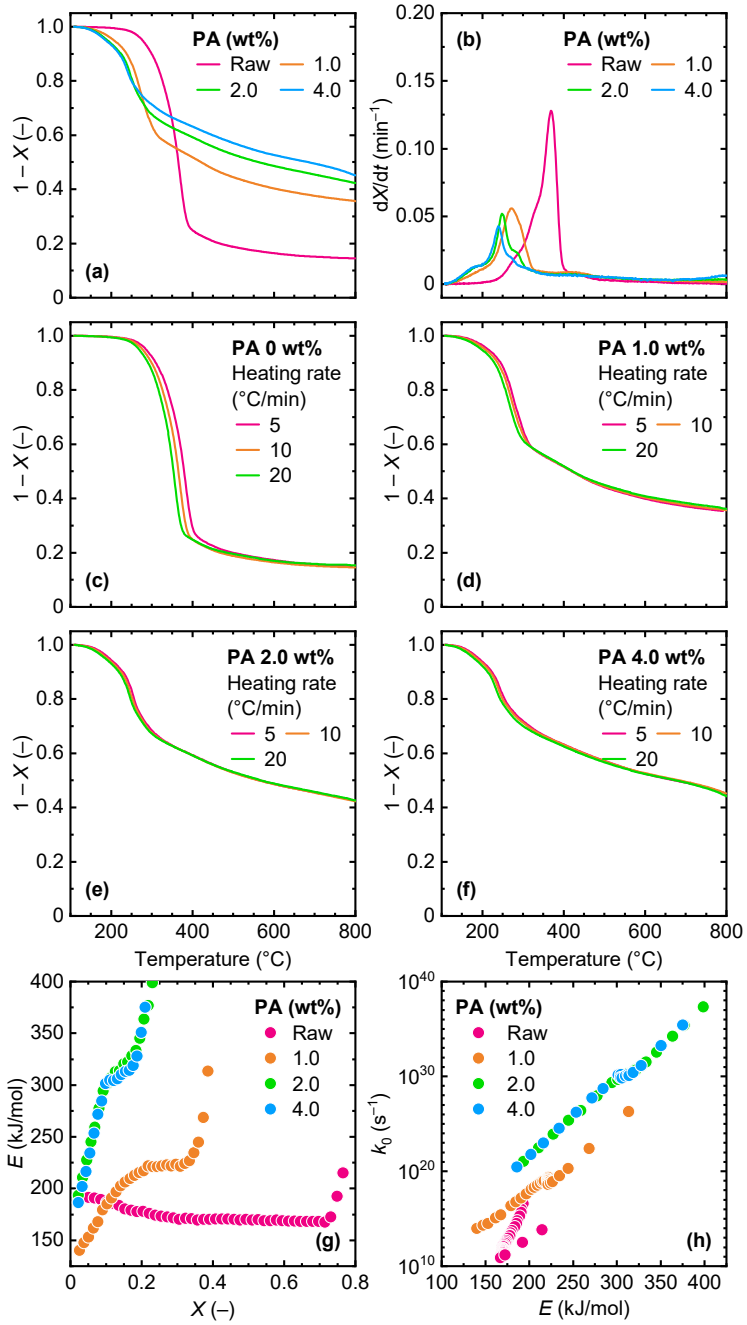

Figure 4. TGA of PA-loaded CD: (**a**,**b**) pyrolysis at 10 °C/min, (**c**–**f**) pyrolysis at 5, 10, or 20 °C/min, and (**g**,**h**) activation energy (*E*) and frequency factor (k_0) analyzed by DAEM.

Kinetic analysis based on DAEM was conducted using data obtained at different heating rates (Figure 4c–f). The activation energy (*E*) and frequency factor (k_0) was calculated at each conversion (*X*) with the interval of 0.02. The results are shown in Figure 4g,h. The kinetic analysis was conducted only for the portions of the pyrolysis curves that showed clear differences depending on the heating rate. As the PA impregnation amount increased, the corresponding range of conversion became narrower, and for PA 2.0 and 4.0 wt%, only the range of $X = 0$–0.2 was analyzed. For raw CD, *E* remained nearly constant (167–193 kJ mol^{-1}) over $X = 0$–0.7. In contrast, PA-loaded CD showed markedly different behavior: *E* was lower in the early stage, reflecting catalytic dehydration, then increased with *X* as volatiles release progressed. For PA = 1.0 wt%, *E* became constant around $X \approx 0.2$ and increased again at higher conversion, likely corresponding to char decomposition into light gases. The result may indicate that the 1.0 wt% sample maintained active dehydration of *X* while allowing volatile evolution over a wide range, favoring anhydrosugars formation. The relationship between *E* and the frequency factor (k_0) followed the

compensation effect [40], where k_0 increased with E, implying relatively homogeneous reaction pathways. Since similar kinetic results were obtained for 2.0 wt% and 4.0 wt% PA samples, 2.0 wt% was considered sufficient to maximize PA activity. The higher k_0 observed for 2.0 wt% compared to 1.0 wt% indicates more abundant active sites. Consequently, the 4.0 wt% sample was excluded from subsequent fluidized-bed experiments.

To further clarify PA's role, model compounds representing biomass components were analyzed (Figure 5). Consistent with previous results [24], cellulose showed a clear response: the peak temperature decreased from 347 °C to 310 °C with the loading of PA, while char yield at 800 °C increased from 5.0 wt% to 16.3 wt%. Thus, only 0.3 wt% of PA, corresponding to 0.095 wt% of P, resulted in the significant differences. In contrast, xylan and lignin exhibited negligible change in decomposition behavior upon PA loading. Lignin is a high-molecular-weight phenolic compound and has a completely different chemical structure from cellulose, whereas xylan is a polysaccharide like cellulose. Therefore, the lack of effect of PA on xylan was unexpected. However, although xylan is a polysaccharide, the main components of its pyrolysis bio-oil are organic acids and furans rather than anhydrosugars, which is different from pyrolysis products of cellulose. It is, therefore, reasonable to conclude that PA loading is particularly effective for promoting anhydrosugar formation. Even in the presence of hemicellulose or lignin, PA may act selectively on cellulose, lowering the pyrolysis temperature and facilitating its conversion to LGO. Nevertheless, because phosphoric acid, which exhibits catalysis similar to PA in cellulose pyrolysis, has been reported to influence the pyrolysis of hemicellulose and lignin as well [41,42], further investigation is required to elucidate the effects of PA on these components.

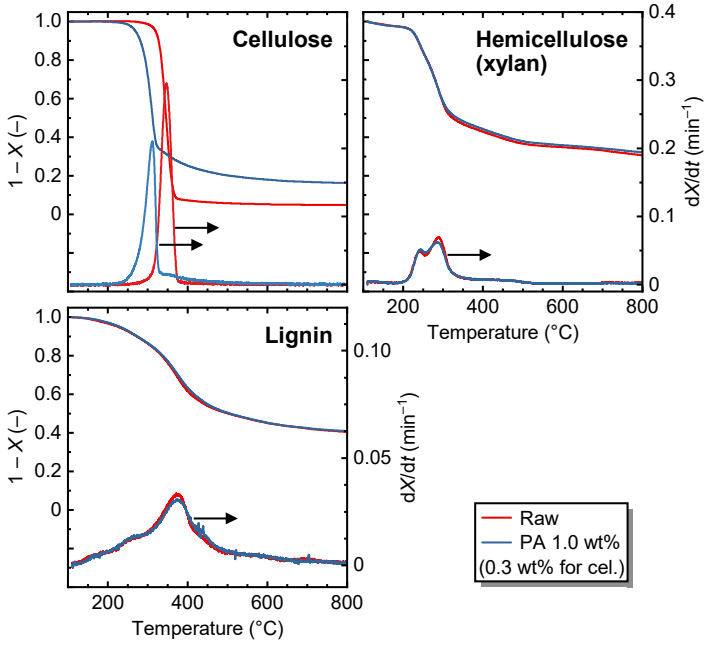

Figure 5. TGA of model compounds with or without PA loading: pyrolysis at 10 °C/min.

3.3. LGO Production in the Fluidized-Bed Pyrolyzer

Continuous pyrolysis of oxalic acid-washed CD loaded with 0–2.0 wt% PA was carried out in the fluidized-bed pyrolyzer. The results are summarized in Table 2. Two operation modes were examined: mode I, where char accumulated in the bed, and mode II, where char and sand were continuously discharged to maintain steady-state operation.

First, mode I pyrolysis was carried out using samples with different reaction temperatures and PA loading levels. The pyrolysis of cellulose occurs at 300–350 °C. To take advantage of the high reaction rate of pyrolysis and enhance productivity, bio-oil production using a fluidized-bed pyrolyzer is generally conducted at 400–500 °C [28]. Accordingly, the initial experiment was conducted at $T_{1,ave}$ of 400 °C (run 1). Under these conditions, the yields of both LGO and LGA were extremely low. One possible reason was that the rapid heating in the fluidized bed caused occurrence of cellulose pyrolysis before PA could diffuse into the CD particles, limiting its catalytic effect. This explanation is consistent with reports showing that in cellulose pyrolysis, excessive heating rates hinder the activity of loaded catalysts [24]. To test this hypothesis, PA-loaded CD (2.0 wt%) was preheated at 150 °C for 1 h under N_2 before pyrolysis to allow catalyst migration (run 2). However, LGO and LGA yields remained minimal.

Table 2. Pyrolysis of CD in the fluidized-bed pyrolyzer.

Run	**1**	**2**	**3**	**4**	**5**	**6**	**7**	**8**	**9**	**10**	**11**	**12**	**13**	**14**
Mode	**I**	**I**	**I**	**I**	**I**	**I**	**I**	**I**	**I**	**I**	**I**	**II**	**II**	**II**
PA content in CD (wt%)														
	2.0	2.0	1.0	1.0	2.0	2.0	2.0	1.0	1.0	1.0	0	1.0	0	1.0
Feeding time (min)														
	30	30	30	30	30		30	30	30	45	38	120	77	30
Measured temperature (°C)														
T_5	383	406	405	273	273	310	363	363	292	286	402	278	273	280
T_4	403	414	413	275	275	313	363	363	297	291	426	283	278	285
T_3	422	422	421	280	280	320	369	369	305	299	452	291	286	293
T_2	442	433	432	283	283	327	377	377	314	308	479	300	295	302
T_1	411	403	402	262	262	302	352	352	301	295	448	287	282	289
$T_{1,ave}$	400	393	396	259	253	297	347	349	297	282	436	295	287	283
Yield (wt%)														
LGA	0	0	1.6	0.03	0.01	0.1	0	0.8	0.2	0.3	11.0	1.4	0.7	1.9
LGO	0.3	0.2	0.2	3.8	2.0	4.1	4.1	4.6	6.3	5.2	0.04	4.2	0.2	5.4
Yield (wt%-cellulose)														
LGA	0	0.0	4.3	0.1	0.04	0.2	0.0	2.1	0.6	0.8	31.0	3.8	1.9	5.2
LGO	0.9	0.5	0.5	10.4	5.5	11.3	11.2	12.7	17.1	14.2	0.1	11.4	0.4	14.8
Peak area ratio (%)														
A	15.8	17.1	22.7	7.5	7.0	8.1	10.6	13.4	9.9	10.4	31.2	14.0	24.8	10.4
F	18.9	16.9	14.8	14.5	16.6	15.7	16.2	11.2	12.8	15.5	3.9	12.2	9.1	9.9
L	48.6	47.6	37.6	22.7	30.5	25.9	29.9	27.6	18.2	19.1	19.0	18.0	23.2	16.3
O	5.8	4.5	8.6	4.8	4.8	3.9	4.2	5.7	5.9	6.1	9.3	8.7	14.6	10.7
S	10.9	14.0	16.4	50.5	41.1	46.4	39.0	41.9	53.2	48.9	36.6	47.1	28.4	52.7
Y_i (–)														
A	1.42	0.96	2.18	0.61	0.36	0.77	1.22	1.98	1.34	1.32	10.14	2.23	2.08	1.76
F	1.69	0.95	1.42	1.18	0.87	1.51	1.86	1.66	1.74	1.97	1.28	1.96	0.76	1.67
L	4.37	2.68	3.62	1.85	1.58	2.48	3.43	4.07	2.48	2.42	6.17	2.87	1.95	2.75
O	0.53	0.25	0.83	0.39	0.25	0.37	0.48	0.85	0.80	0.78	3.03	1.39	1.22	1.80
S [1]	0.63	0.62	1.38	0.30	0.12	0.31	0.37	1.54	0.96	0.99	11.85	3.37	2.23	3.50
Gas yield (wt%)														
H_2 ($\times 10^{-6}$)										1.40		4.36	6.35	
CO										0.11		0.76	0.05	
CO_2										2.27		2.42	1.24	
Char yield (wt%)														
total										58.6		54.4	74.0	60.0
(reactor)												35.7	64.9	50.9
(char collector)												18.5	9.1	9.3

[1] S does not include LGO.

When PA loading was reduced to 1.0 wt% (run 3), the LGO yield remained low, but LGA yield improved slightly to 1.6 wt% (4.3 wt% on a cellulose basis). In contrast, pyrolysis of PA-free CD (run 11) produced LGA selectively, achieving 31 wt% (cellulose basis) in 30 min continuous operation, which was much higher than the LGA yield, reported in the literature [30], from CD without acid-washing pretreatment in the fluidized-bed pyrolysis under similar conditions. According to TGA results, 1.0 wt% PA was insufficient to fully express catalytic activity; thus, the LGA formed in run 3 likely originated from non-catalyzed cellulose pyrolysis. In other words, it is considered that in runs 1–3, PA was active for converting overall or a portion of cellulose into LGO; however, it was in practice not obtained in the bio-oil.

The difference between LGA and LGO was considered in terms of their thermal stability in the gas phase. LGA is known to be relatively stable even at high temperature. Fukutome et al. reported that nearly 100% of LGA could be recovered after treatment at 400 °C for 1.4 s [43]. At even higher temperatures, however, it underwent decomposition and gasification. Because of this, in biomass pyrolysis for LGA production, a residence time of less than 1 s at around 500 °C is recommended [27]. For LGO, previous pyrolysis studies have also reported a decrease in yield with increase in temperature [26], but no quantitative evaluation has yet been conducted. To clarify this, the gas-phase thermal stability of LGO was examined (Figure 6). The recovery of LGO remained quantitative at 200 °C but declined rapidly above 300 °C, where nearly 90% of LGO decomposed or polymerized at 400 °C, even with a residence time of only ≈1 s. This represents the first quantitative demonstration of LGO's thermal instability in the gas phase and highlights the critical importance of temperature control during continuous pyrolysis. In slow heating fixed bed systems, LGO starts to form under conditions, where the whole reactor is still at low temperatures, <300 °C. Therefore, the thermal stability of LGO does not become an issue. However, in

continuous feeding systems such as fluidized beds, the feedstock enters an already hot environment, leading to extensive LGO deterioration unless the bed temperature is optimized.

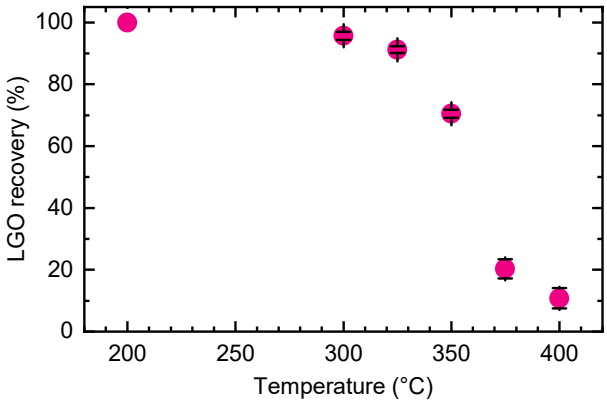

Figure 6. LGO recovery in the thermal treatment of LGO in the flow-type reactor at 200–400 °C for 1.2–1.7 s.

Based on these findings, subsequent runs were performed at $T_{1,ave}$ < 400 °C (runs 4–10). As shown in Table 2, for both PA loadings of 1.0 and 2.0 wt%, LGO yield drastically increased. Figure 7 compares the LGO yields under each condition. The maximum LGO yield was achieved when $T_{1,ave}$ was around 300 °C (runs 6 and 9). At lower temperatures (runs 4 and 5), pyrolysis likely did not proceed sufficiently, while at higher temperatures, as mentioned earlier, the yield decreased due to gas-phase reactions of LGO. The residence time of volatiles in the headspace, estimated from the carrier gas flow rate, was 8.7–11.2 s, which was long enough at high temperature for LGO to decompose or undergo polycondensation. Comparing PA 1.0 wt% and 2.0 wt%, the former produced a higher LGO yield. This suggests that 2.0 wt% PA was excessive, leading to pronounced charring that inhibited LGO formation. The maximum LGO yield obtained in this study was 6.3 wt% (run 9), corresponding to 17.1 wt% on a cellulose basis. This yield is comparable to those reported for screw-conveyor-type pyrolysis systems, demonstrating that similar performance can be achieved even in a fluidized-bed pyrolyzer using PA, a biorenewable catalyst. However, even at this temperature range, some loss of LGO likely occurred through gas-phase reactions in the headspace. This indicates that primary pyrolysis occurring in the fluidized bed produced LGO at higher yields. Moreover, PA loading of 1.0 wt% appeared insufficient since LGA was detected, suggesting that an optimum lies between 1.0 and 2.0 wt%. From these results, further improvement in LGO yield can be expected through reactor design for shorter residence time of volatiles in gas-phase and optimization of PA loading amount.

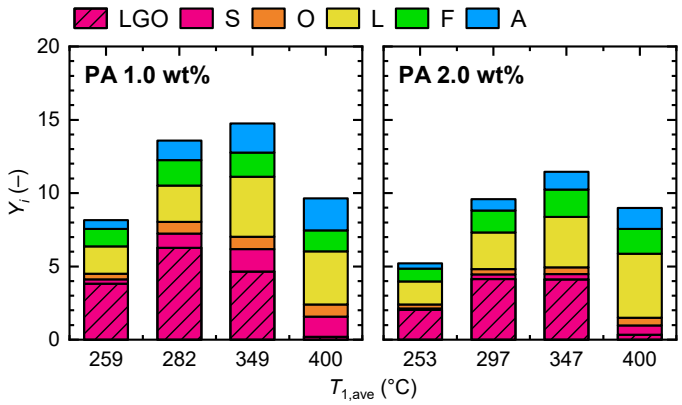

Figure 7. Semi-quantitative yield of each compound group, Y_i, in runs 1 and 3–9: (**left**) PA 1.0 wt% and (**right**) PA 2.0 wt%. Ys does not include LGO. The yield of LGO is presented separately.

The relative peak areas of GC-MS-detected compounds are summarized in Table 2, and their semi-quantitative yields (Y_i) are shown in Figure 7. Supplementary Material presents detailed compositions of representative bio-oils (Table S1) and their chromatograms (Figure S1). At low bed temperatures ($T_{1,ave}$ < 350 °C), the S fraction accounted for 39–50% of the total peak area. The S group was dominated by LGO (75–95%), followed by LGA and DGP. In most runs, 4-propyl guaiacol was the major component among A, furfural among F, and acetic acid among L. The "L" fraction also contained terpenoid compounds such as ferruginol, whereas O included silicon- or nitrogen-containing compounds. As indicated by TGA results, PA showed negligible catalytic

effects on hemicellulose and lignin; hence, furans and aromatics formed primarily via non-catalytic pyrolysis at low temperatures, with their yields increasing at higher $T_{1,ave}$. At elevated temperatures (runs 1–3), the large fraction of L may suggest that vapor-phase degradation of LGO occurred, yielding related low molecular-weight species.

Figure 8 illustrates the temperature profiles (T_1–T_5) observed during run 10, where relatively high LGO yields were obtained. Initially, T_2 (<100 mm above the static bed surface) was slightly higher than T_1 (within the bed), while T_3–T_5 decreased progressively along the distance from the bed. This trend was consistent across all runs (see Table 2). The lower T_1 relative to T_2 likely reflects the position of the bed within furnace B and local heat convection effects. During operation, T_1 decreased sharply, by about 20 °C, immediately after CD feeding began, and then gradually increased as the run progressed. This temperature drop is attributed to the endothermic nature of pyrolysis and the cooling effect of volatiles generation. T_2 decreased steadily toward the end of feeding, suggesting that the extent of pyrolysis increased over time. The continuous increase in CO_2 flow rate at the reactor outlet with time (Figure 9) supports this interpretation. It is thought that the reaction rate of pyrolysis was low due to the low temperature of fluidized bed, while the feeding rate of CD was high, leading to the decrease in T_2 with operation time.

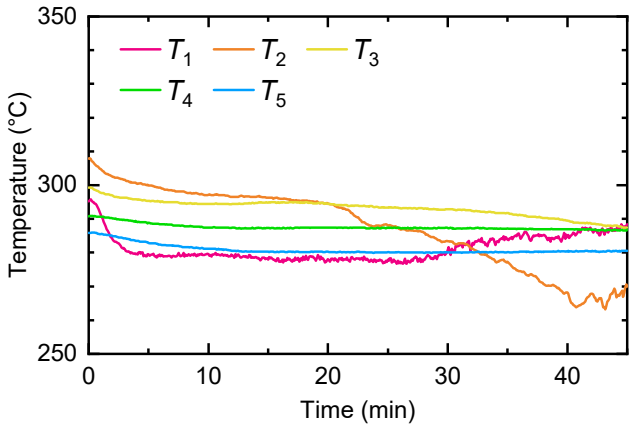

Figure 8. Changes in temperature inside the reactor monitored at different positions, T_1–T_5, during run 10.

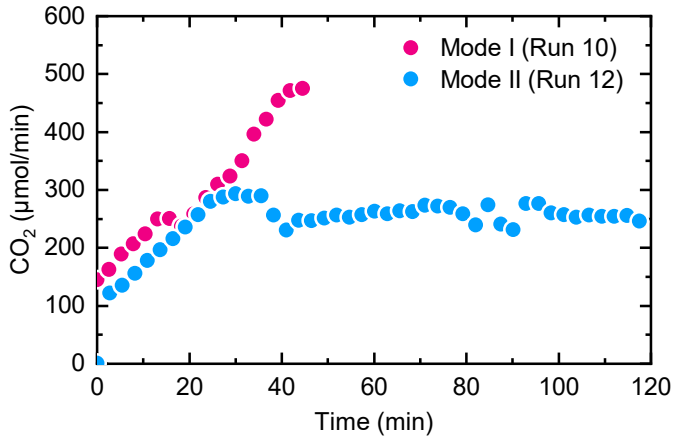

Figure 9. Flow rate of CO_2 produced during runs 10 and 12. Runs 10 and 12 employed different modes and feed times, but all other reaction conditions, including the set temperature and feedstock, were identical.

To achieve steady-state operation, mode II experiments (runs 12–14) were conducted, where char and sand were continuously withdrawn from the reactor. Char discharge began 10–15 min after the start of CD feeding. The average bed temperature was maintained around 290 °C. For raw CD (run 13), the low temperature resulted in incomplete pyrolysis, yielding negligible LGO and LGA with high char yield. In contrast, PA-loaded CD produced LGO selectively, similar to mode I. The CO_2 evolution profile (Figure 9) for run 12 indicates that steady-state operation was reached after approximately 30 min of continuous feeding, where the CO_2 flow rate reached plateau. Meanwhile, based on Figure 9, the steady-state was not established in run 14 due to the short feeding time.

The LGO yield in run 12 was 11.4 wt%-cellulose, lower than in run 14 and lower than in the best mode I runs (9–10). Two main factors may explain this. First, in steady-state operation, part of the biomass can be discharged before completion of pyrolysis, causing loss of LGO. Extending the residence time of CD in the bed, by

decreasing the sand feeding rate, would mitigate this effect. Second, interactions between volatile compounds and char could influence LGO formation. Two primary pathways for LGO formation during pyrolysis are present [8]. The first involves the direct catalysis of PA on cellulose in CD. PA or the phosphoric acid formed through its hydrolysis [24] promotes the dehydration of cellulose, thereby facilitating LGO formation. Past studies have reported on the catalytic mechanism of phosphoric acid [22]. The second pathway is the conversion of anhydrosugars, including LGA, formed during non-catalytic pyrolysis into LGO over solid catalysts. For the second pathway, char may exert both positive and negative effects. Ye et al. reported that phosphorus-containing char derived from phosphoric acid-impregnated biomass can catalytically convert volatiles of biomass pyrolysis, LGA and related oligomers in particular, into LGO [13]. This implies that char in the fluidized bed of the present study may also act as a secondary catalyst. Thus, LGO formation could proceed via both direct pyrolysis of CD and char-mediated reforming of volatile intermediates. In mode I, where char accumulated in the bed, such catalytic activity might have enhanced LGO yield. However, prolonged operation (e.g., run 10 versus run 9) showed that LGO yield decreased with time, suggesting that aged char also promotes LGO decomposition or coking. As aforementioned, because LGA chemically interacts with char, it is required for achieving its high yield during pyrolysis to suppress the contact between them. The same can be considered true for LGO. This dual role implies the importance for the bed to contain only fresh char as much as possible. Increasing the sand feed rate relative to CD may help satisfy this requirement, maximizing beneficial catalytic effects while minimizing deactivation and LGO loss.

In summary, this study demonstrated that selective and continuous production of LGO from PA-loaded CD is achievable using a fluidized-bed pyrolyzer. The obtained yield was comparable to that reported for the commercial LGO production process [8] and for laboratory-scale continuous LGO production using a screw-conveyor pyrolyzer [26]. In addition, the thermal stability of LGO and its interaction with char revealed in this study suggest that the yield could be further improved through reactor designs that account for LGO stability and through optimization of the feeding rate balance between the biomass and the bed material. However, challenges must be addressed before practical application of the proposed method can be realized. In this study, CD was subjected to oxalic acid washing and PA loading as pretreatments. Oxalic acid is consumed during acid washing; therefore, an appropriate acidic solution should be selected based on AAEM-removal efficiency and the cost per quantity of the acid. Because a drying step is unavoidable, it is also necessary to determine how much the LGO yield decreases when acid washing is omitted. As suggested by fundamental fixed-bed pyrolysis experiments, acid-washing has a substantial effect on LGA formation. Nevertheless, in the case of LGO, previous studies have shown that the efficient production can be achieved by directly loading biomass with phosphoric acid without acid washing, indicating that high yields may also be attainable with PA loading alone. Regarding PA loading, the impregnation with aqueous solution, used in this study, requires a drying step, which is energy intensive. To reduce the energy demand, it is required to investigate whether comparable PA loading can be achieved by alternative methods such as paste blending or spray impregnation. Similar to phosphoric acid and other liquid catalysts, PA is essentially consumed during pyrolysis, and thus catalyst cost becomes pronounced. Because PA is currently more expensive than phosphoric acid, measures to reduce the cost are required. As discussed in our previous work [24], using partially refined materials derived from grains, such as defatted rice bran, rather than pure PA may reduce costs. Another possibility is to recover and regenerate phosphorus contained in the discharged char as phosphoric acid or other reusable forms. In fluidized-beds, char is discharged together with the bed material; thus, char separation and recovery represent another important issue. Furthermore, the experiments in this study were conducted at a small scale, with a biomass feed rate of only 0.5 g/min. Scale-up affects mass and heat transfer and may consequently alter product yields, making scale-up studies indispensable for practical implementation.

4. Conclusions

This study demonstrated the continuous production of LGO from woody biomass using a fluidized-bed pyrolyzer combined with a biogenic phosphorus catalyst, PA. Within the range of experimental conditions examined in this work, the following conclusions were drawn:

(1) Oxalic acid-washing effectively removed AAEMs, such as K, Mg, and Ca, from CD. The removal was not complete, but it was sufficient to drastically improve anhydrosugars yield during the pyrolysis. The fixed-bed pyrolysis study also found that comparable LGA yields can be obtained even when CO_2 was used as the carrier gas instead of N_2, and that performing the pyrolysis under reduced pressure was not necessary.

(2) In TGA, kinetic parameters of pyrolysis were greatly altered by the PA loading. PA selectively catalyzed cellulose pyrolysis, while pyrolysis of hemicellulose and lignin remained unchanged. The temperature of maximum pyrolysis reaction rate decreased from 369 °C for raw CD to 239 °C for PA 4.0 wt% by the catalysis.

(3) Continuous pyrolysis experiments revealed a strong dependence of LGO yield on temperature and PA loading. At high temperatures ($T_{1,ave} \approx 400$ °C), LGO degraded rapidly in the gas phase, as confirmed by the separate thermal stability tests showing 90% loss within 1.2 s at 400 °C. Consequently, optimal LGO production was achieved at lower temperatures ($T_{1,ave} \approx 300$ °C), where gas-phase degradation was suppressed. The maximum LGO yield reached 6.3 wt% (17.1 wt%-cellulose) in mode I, which was comparable to values reported for screw-conveyor using mineral acid catalysts with high loadings.

(4) The pyrolysis study indicated both positive and negative influence of char accumulated in the bed. P-containing char from PA-loaded CD may act as a secondary catalyst, converting intermediates, such as LGA and oligomers, into LGO. However, as operation proceeds, char undergoes deactivation by coking and convert LGO into lighter compounds or coke. Maintaining a moderate concentration of fresh, catalytically active char is therefore required for improving the yield during steady-state operation. Adjusting the feed rates of biomass and sand would provide a means to control residence time and char renewal in the reactor.

In summary, this work explores a new route for sustainable LGO production through fluidized-bed pyrolysis using a biogenic catalyst. Further improvements in reactor design, catalyst distribution, and temperature control could enable higher yields and scalability. These findings contribute to the broader development of catalytic systems for converting lignocellulosic biomass into valuable chemicals.

Supplementary Materials

The additional data and information can be downloaded at: https://media.sciltp.com/articles/others/251127135 6338802/RC-25100048-Author-Supplementary_Material_revised-V2.pdf. Figure S1. GC-MS chromatograms of bio-oils. Table S1. Compounds detected in GC-MS analysis for representative bio-oils. Runs 1, 9, 12, and 14 are bio-oils recovered at the cold trap. The bio-oil at the cold trap contained more L, compared to that recovered at the filter trap. The latter was more abundant in LGO due to its tendency to form aerosols. Runs 10 and 11 are mixture of bio-oils recovered at the two traps. Main components: (a) acetic acid, (b) furfural, (c) LGO, (d) DGP, (e) 4-propyl guaiacol, (f) LGA, and (g) ferruginol. Table S2 List of symbols and acronyms.

Author Contributions

T.N.R.: conceptualization, formal analysis, investigation, writing—original draft preparation; S.K.: conceptualization, methodology, funding acquisition, project administration, visualization, writing—review & editing; C.A.: investigation, R.A.: investigation, Y.H.: data curation, investigation; J.-i.H.: supervision, writing—review & editing. All authors have read and agreed to the published version of the manuscript.

Funding

This work was funded by a project (JPNP16002) subsidized by the New Energy and Industrial Technology Development Organization (NEDO).

Institutional Review Board Statement

Not applicable.

Informed Consent Statement

Not applicable.

Data Availability Statement

The original contributions presented in the study are included in the article. Further inquiries can be directed to the corresponding author.

Acknowledgments

The authors acknowledge “Crossover Alliance to Create the Future with People, Intelligence and Materials” from MEXT, Japan, and KUMA Science Engineering and Culture Promotional Foundation for their research support.

Conflicts of Interest

Given the role as an editorial board member of Renewable Chemistry, Shinji Kudo had no involvement in the peer review of this paper and had no access to information regarding its peer-review process. Full responsibility for the editorial process of this paper was delegated to another editor of the journal.

Use of AI and AI-Assisted Technologies

During the preparation of this work, the authors used ChatGPT to improve the readability and language. After using this tool/service, the authors reviewed and edited the content as needed and takes full responsibility for the content of the published article.

References

1. Lee, R.A.; Lavoie, J.-M. From first- to third-generation biofuels: Challenges of producing a commodity from a biomass of increasing complexity. *Anim. Front.* **2013**, *3*, 6–11. https://doi.org/10.2527/af.2013-0010.
2. Hayashi, J.-i. Roles of Forests and Forest-Resource Conversion in Societies with Carbon Resource Regeneration and Storage. Chemical Engineering of Japan. 2025; Volume 89, pp. 15–18. Available online: https://service.kktcs.co.jp/smms2/member/journal_search/Download.htm?dummy=0&file=Bulletin089070351.pdf (accessed on 26 November 2025).
3. Endo, S.; Aizawa, N. Annual Energy Reviews-2018. *Enermix* **2019**, *98*, 454–455. https://doi.org/10.20550/jieenermix.98.5_454.
4. Warne, C.M.; Fadlallah, S.; Whitwood, A.C.; et al. Levoglucosenone-derived synthesis of bio-based solvents and polyesters. *Green. Chem. Lett. Rev.* **2022**, *16*, 2154573. https://doi.org/10.1080/17518253.2022.2154573.
5. Tsai, Y.H.; Borini Etichetti, C.M.; Cicetti, S.; et al. Design, synthesis and evaluation of novel levoglucosenone derivatives as promising anticancer agents. *Bioorg Med. Chem. Lett.* **2020**, *30*, 127247. https://doi.org/10.1016/j.bmcl.2020.127247.
6. Camp, J.E. Bio-available Solvent Cyrene: Synthesis, Derivatization, and Applications. *ChemSusChem* **2018**, *11*, 3048–3055. https://doi.org/10.1002/cssc.201801420.
7. Liu, X.; Carr, P.; Gardiner, M.G.; et al. Levoglucosenone and Its Pseudoenantiomer iso-Levoglucosenone as Scaffolds for Drug Discovery and Development. *ACS Omega* **2020**, *5*, 13926–13939. https://doi.org/10.1021/acsomega.0c01331.
8. Kudo, S.; Huang, X.; Asano, S.; et al. Catalytic Strategies for Levoglucosenone Production by Pyrolysis of Cellulose and Lignocellulosic Biomass. *Energy Fuels* **2021**, *35*, 9809–9824. https://doi.org/10.1021/acs.energyfuels.1c01062.
9. Kudo, S.; Zhou, Z.; Norinaga, K.; et al. Efficient levoglucosenone production by catalytic pyrolysis of cellulose mixed with ionic liquid. *Green. Chem.* **2011**, *13*, 3306–3311. https://doi.org/10.1039/c1gc15975e.
10. Meng, X.; Zhang, H.; Liu, C.; et al. Comparison of Acids and Sulfates for Producing Levoglucosan and Levoglucosenone by Selective Catalytic Fast Pyrolysis of Cellulose Using Py-GC/MS. *Energy Fuels* **2016**, *30*, 8369–8376. https://doi.org/10.1021/acs.energyfuels.6b01436.
11. Saragai, S.; Kudo, S.; Sperry, J.; et al. Catalytic deep eutectic solvent for levoglucosenone production by pyrolysis of cellulose. *Bioresour. Technol.* **2022**, *344*, 126323. https://doi.org/10.1016/j.biortech.2021.126323.
12. Li, K.; Wang, B.; Bolatibieke, D.; et al. Catalytic fast pyrolysis of biomass with Ni-P-MCM-41 to selectively produce levoglucosenone. *J. Anal. Appl. Pyrolysis* **2020**, *148*, 104824. https://doi.org/10.1016/j.jaap.2020.104824.
13. Ye, X.-n.; Lu, Q.; Wang, X.; et al. Catalytic Fast Pyrolysis of Cellulose and Biomass to Selectively Produce Levoglucosenone Using Activated Carbon Catalyst. *ACS Sustain. Chem. Eng.* **2017**, *5*, 10815–10825. https://doi.org/10.1021/acssuschemeng.7b02762.
14. Wang, Z.; Lu, Q.; Zhu, X.F.; et al. Catalytic fast pyrolysis of cellulose to prepare levoglucosenone using sulfated zirconia. *ChemSusChem* **2011**, *4*, 79–84. https://doi.org/10.1002/cssc.201000210.
15. Xu, A.; Huang, X.; Tang, G.; et al. Levoglucosenone production by catalytic fast pyrolysis of cellulose mixed with alkali metal-doped Keggin heterpolyacid salt. *Fuel Process Technol.* **2023**, *242*, 107609. https://doi.org/10.1016/j.fuproc.2022.107609.
16. A, L.; Radhakrishnan, H.; Hu, H.; et al. Plasma electrolysis of cellulose in polar aprotic solvents for production of levoglucosenone. *Green. Chem.* **2020**, *22*, 7871–7883, Article. https://doi.org/10.1039/d0gc02813d.
17. Cao, F.; Schwartz, T.J.; McClelland, D.J.; et al. Dehydration of cellulose to levoglucosenone using polar aprotic solvents. *Energy Environ. Sci.* **2015**, *8*, 1808–1815. https://doi.org/10.1039/c5ee00353a.
18. Huang, X.; Kudo, S.; Asano, S.; et al. Improvement of levoglucosenone selectivity in liquid phase conversion of cellulose-derived anhydrosugar over solid acid catalysts. *Fuel Process Technol.* **2021**, *212*, 106625. https://doi.org/10.1016/j.fuproc.2020.106625.
19. Milescu, R.A.; Segatto, M.L.; Stahl, A.; et al. Sustainable Single-Stage Solid–Liquid Extraction of Hesperidin and Rutin from Agro-Products Using Cyrene. *ACS Sustain. Chem. Eng.* **2020**, *8*, 18245–18257. https://doi.org/10.1021/acssuschemeng.0c06751.
20. Dobele, G.; Dizhbite, T.; Rossinskaja, G.; et al. Pre-treatment of biomass with phosphoric acid prior to fast pyrolysis. *J. Anal. Appl. Pyrolysis* **2003**, *68–69*, 197–211. https://doi.org/10.1016/s0165-2370(03)00063-9.

21. Dobele, G.; Rossinskaja, G.; Telysheva, G.; et al. Cellulose dehydration and depolymerization reactions during pyrolysis in the presence of phosphoric acid. *J. Anal. Appl. Pyrolysis* **1999**, *49*, 307–317. https://doi.org/10.1016/s0165-2370(98)00126-0.
22. Wang, B.; Li, K.; Zhang, C.-b.; et al. Selective production of levoglucosenone from catalytic pyrolysis of regenerated cellulose from a H_3PO_4-H_2O system. *Ind. Crops Prod.* **2023**, *206*, 117594. https://doi.org/10.1016/j.indcrop.2023.117594.
23. Ung, S.P.M.; Li, C.-J. From rocks to bioactive compounds: A journey through the global P(v) organophosphorus industry and its sustainability. *RSC Sustain.* **2023**, *1*, 11–37. https://doi.org/10.1039/d2su00015f.
24. Rafenomananjara, T.N.; Kudo, S.; Sperry, J.; et al. Phytic acid as a biorenewable catalyst for cellulose pyrolysis to produce levoglucosenone. *RSC Sustain.* **2025**, *3*, 1366–1375. https://doi.org/10.1039/d4su00502c.
25. Court, G.R.; Lawrence, C.H.; Raverty, W.D.; et al. Method for Converting Lignocellulosic Materials into Useful Chemicals. WO 2011/000030 A1, 6 January 2011.
26. Dobele, G.; Zhurinsh, A.; Volperts, A.; et al. Study of levoglucosenone obtained in analytical pyrolysis and screw-type reactor, separation and distillation. *Wood Sci. Technol.* **2020**, *54*, 383–400. https://doi.org/10.1007/s00226-020-01164-7 Scopus.
27. Itabaiana Junior, I.; do Nascimento, A.M.; de Souza, R.O.M.A.; et al. Levoglucosan: A promising platform molecule? *Green. Chem.* **2020**, *22*, 5859–5880. https://doi.org/10.1039/d0gc01490g.
28. Rover, M.R.; Aui, A.; Wright, M.M.; et al. Production and purification of crystallized levoglucosan from pyrolysis of lignocellulosic biomass. *Green. Chem.* **2019**, *21*, 5980–5989. https://doi.org/10.1039/c9gc02461a.
29. Patwardhan, P.R.; Dalluge, D.L.; Shanks, B.H.; et al. Distinguishing primary and secondary reactions of cellulose pyrolysis. *Bioresour. Technol.* **2011**, *102*, 5265–5269. https://doi.org/10.1016/j.biortech.2011.02.018.
30. Yoshimura, K.; Kaku, A.; Hachiyama, Y.; et al. Preparation of levoglucosan-rich bio-oil and its application to alkaline hydrothermal conversion of CO_2 to formic acid. *Tetsu-Hagané* **2025**, *111*, 917–925 https://doi.org/10.2355/tetsutohagane.TETSU-2025-021.
31. Cao, F.; Xia, S.; Yang, X.; et al. Lowering the pyrolysis temperature of lignocellulosic biomass by H_2SO_4 loading for enhancing the production of platform chemicals. *Chem. Eng. J.* **2020**, *385*, 123809. https://doi.org/10.1016/j.cej.2019.123809.
32. Sluiter, A.; Hames, B.; Ruiz, R.; et al. *Determination of Ash in Biomass*; Technical Report NREL/TP-510-42622; NREL: Golden, CO, USA, 2008.
33. Miura, K.; Maki, T. A Simple Method for Estimating f(E) and k0(E) in the Distributed Activation Energy Model. *Energy Fuels* **1998**, *12*, 864–869. https://doi.org/10.1021/ef970212q.
34. Wei, F.; Kudo, S.; Asano, S.; et al. Staged Pyrolytic Conversion of Acid-Loaded Woody Biomass for Production of High-Strength Coke and Valorization of Volatiles. *Energy Fuels* **2022**, *36*, 6949–6958. https://doi.org/10.1021/acs.energyfuels.2c01352.
35. Wang, W.; Lemaire, R.; Bensakhria, A.; et al. Review on the catalytic effects of alkali and alkaline earth metals (AAEMs) including sodium, potassium, calcium and magnesium on the pyrolysis of lignocellulosic biomass and on the co-pyrolysis of coal with biomass. *J. Anal. Appl. Pyrolysis* **2022**, *163*, 105479. https://doi.org/10.1016/j.jaap.2022.105479.
36. Amenaghawon, A.N.; Ayere, J.E.; Amune, U.O.; et al. A comprehensive review of recent advances in the applications and biosynthesis of oxalic acid from bio-derived substrates. *Environ. Res.* **2024**, *251*, 118703. https://doi.org/10.1016/j.envres.2024.118703.
37. Kiyozumi, T.; Kudo, S.; Mori, A.; et al. Synthesis of Oxalate from CO_2 and Cesium Carbonate Supported Over Porous Carbon. *ISIJ Int.* **2022**, *62*, 2476–2482. https://doi.org/10.2355/isijinternational.ISIJINT-2022-159.
38. Słupianek, A.; Dolzblasz, A.; Sokołowska, K. Xylem Parenchyma—Role and Relevance in Wood Functioning in Trees. *Plants* **2021**, *10*, 1247. https://doi.org/10.3390/plants10061247.
39. Zhao, L.; Fu, H.; Xia, Y.-g.; et al. Coproduction of 1,4:3,6-Dianhydro-α-d-glucopyranose, Furfural, and Formic Acid through Oxalic Acid-Assisted Staged Fast Pyrolysis of Cellulose. *Energy Fuels* **2024**, *38*, 4302–4311. https://doi.org/10.1021/acs.energyfuels.3c04958.
40. Czajka, K.; Kisiela, A.; Moroń, W.; et al. Pyrolysis of solid fuels: Thermochemical behaviour, kinetics and compensation effect. *Fuel Process Technol.* **2016**, *142*, 42–53. https://doi.org/10.1016/j.fuproc.2015.09.027.
41. Xie, W.-l.; Hu, B.; Yang, X.; et al. Phosphoric acid catalytic mechanism in lignin pyrolysis: Phosphoric-acid-assisted hydrogen transfer for the decomposition of β-O-4 linkage. *Proc. Combust. Inst.* **2024**, *40*, 105580. https://doi.org/10.1016/j.proci.2024.105580.
42. Nowakowski, D.J.; Woodbridge, C.R. Jones, J.M. Phosphorus catalysis in the pyrolysis behaviour of biomass. *J. Anal. Appl. Pyrolysis* **2008**, 83, 197–204. https://doi.org/10.1016/j.jaap.2008.08.003.
43. Fukutome, A.; Kawamoto, H.; Saka, S. Processes forming Gas, Tar, and Coke in Cellulose Gasification from Gas-Phase Reactions of Levoglucosan as Intermediate. *ChemSusChem* **2015**, *8*, 2240–2249. https://doi.org/10.1002/cssc.201500275.